Available online at www.sciencedirect.com
ScienceDirect
International Journal of Thermal Sciences 45 (2006) 1073–1083
International Journal of Thermal Sciences
www.elsevier.com/locate/ijts

Single-phase liquid friction factors in microchannels ☆

Mark E. Steinke *, Satish G. Kandlikar

Thermal Analysis and Microfluidics Laboratory, Mechanical Engineering Department, Kate Gleason College of Engineering, Rochester Institute of Technology, 76 Lomb Memorial Dr., Rochester, NY 14623, USA

Received 10 September 2005; accepted 30 January 2006

Available online 9 March 2006

Abstract

The validity of friction factor theory based upon conventional sized passages for microchannel flows is still an active area of research. Several researchers have reported significant deviation from predicted values, while others have reported general agreement. The discrepancies in literature need to be addressed in order to generate a set of design equations to predict the pressure drop occurring in microchannel flow devices.

The available literature on single-phase liquid friction factors in microchannels is reviewed. A database is generated to critically evaluate the experimental data available in the literature. An in-depth comparison of previous experimental data is performed to identify the discrepancies in reported literature. It is concluded that the conventional Stokes and Poiseuille flow theories apply for single-phase liquid flow in microchannel flows.

New experimental data is presented and the pressure drop components are carefully analyzed. The developed procedure properly identifies the components of total pressure drop that allow for improved agreement with conventional theory.

Keywords: Microchannel; Single-phase; Pressure drop; Friction factor; Liquid

1. Introduction

The use of microchannel flow passages is becoming more common in a number of industrial applications. The heat and mass transfer enhancements from the small diameter passages is well documented and often relied upon in a practical system.

Kandlikar and Grande [1,2] describe the fabrication techniques and possible trends in microchannels. They remark that the fluid flow in microchannels is further reaching than just efficient heat transfer. It could open up completely new fields not possible only a few years ago.

Steinke and Kandlikar [3] identified single-phase heat transfer enhancement techniques for use in microchannels and minichannels. They speculate that this increase in heat transfer performance from these techniques could place a single-phase liquid system in competition with a two-phase system; thus simplifying the over all complexity and reliability. However, they point out that the added pressure drop resulting from the techniques should be carefully evaluated.

Therefore, it is important to evaluate the predictive methods for pressure drop occurring in a microchannel heat exchanger (MCHX). The design of supporting equipment such as the fluid pump and the secondary heat exchanger require an accurate estimate of the pressure drop in the MCHX.

Unfortunately, the validity of the conventional fluid flow theories in microchannel fluid flows is still disputed. There are experimental data sets that support both sides of the argument. There is a great need to reconcile the discrepancies in the experimental data and determine if the conventional theory applies or if there needs to be new fundamental flow theories formulated especially for microchannel flow passages.

Therefore, a database containing available experimental data for single-phase liquid flow in microchannels is generated. The discrepancies and deviations in the data are identified and classified. Specific experiments under carefully controlled condi-

☆ A preliminary version of this paper was presented at ICMM05: Third International Conference on Microchannels and Minichannels, held at University of Toronto, June 13–15, 2005, organized by S.G. Kandlikar and M. Kawaji, CD-ROM Proceedings, ISBN: 0-7918-3758-0, ASME, New York.

* Corresponding author currently at: IBM Corporation, Systems & Technology Group, Dept. 6T6A/Bldg. 060, 3039 Cornwallis Rd., Research Triangle Park, NC 27709, USA. Tel.: +1 (919) 254 9944; fax: +1 (919) 254 8826.
E-mail address: msteinke@us.ibm.com (M.E. Steinke).

1290-0729/$ – see front matter
doi:10.1016/j.ijthermalsci.2006.01.016

Nomenclature

a	channel width	m
a_i	variable used to calculate parameter p	
A	area	m^2
b	channel height	m
B	bias error	
C^*	normalized Poiseuille number	
D_h	hydraulic diameter $= 4A_c/P_w$	m
e	roughness height	m
f	friction factor	
G	mass flux	$kg\,m^{-2}\,s^{-1}$
K	loss coefficient	
L	channel length	m
L_h	hydrodynamic entrance length	m
L^+	non-dimensional entrance length	
m	exponent used in Eq. (10) $= -0.58$ for present work	
N	number of samples	
p	pressure; parameter	Pa
P	wetted perimeter	m
Po	Poiseuille number, $= f^*Re$	
P_w	wetted perimeter	m
Q	volumetric flow rate	$m^3\,s^{-1}$
r_h	hydraulic radius	m
Re	Reynolds number	
u_{ai}	uncertainty of variable a_i	
U	total uncertainty	
$\overline{V}$	mean velocity	$m\,s^{-1}$
x	axial location	m
x^+	non-dimensional flow distance	

Greek

α_c	channel aspect ratio $= a/b$	
Δ	change in	
κ	Hagenbach factor	
μ	viscosity	$N\,s\,m^{-2}$
θ	side wall angle	degrees
ρ	density	$kg\,m^{-3}$
σ	standard deviation	
τ_w	wall shear stress	Pa

Subscripts

app	apparent
b	bulk or mean
c	cross section
cp	constant property
exp	experimental
FD	fully developed
i	inlet
o	outlet
tot	total
w	wall

tions are conducted to identify the pressure drop components. This is followed by destructive inspection of the microchannels to determine the deviations from prescribed geometry during the microfabrication process. Finally, the conclusions based on the extensive literature review and new experimental data obtained in this study are presented.

2. Literature review of experimental data

The available literature contains over 150 papers that directly deal with the pressure drop measurements in microchannels. For the present study, the papers containing experimental data are reviewed in depth. There are approximately 40 papers that report the detailed experimental data.

In many papers, the authors report data for several different hydraulic diameters. If a single occurrence of a diameter is considered to be an individual data set, there are approximately 220 data sets altogether in the papers that have been reviewed. The total number of data points is over 5,000. The total number of data sets and data points can be used to normalize the respective quantities.

It is important to know what is included in the database to determine the distribution of the data. The most common range of hydraulic diameters and the most data points both are in the 100–200 μm. Fig. 1 shows the percentage of data sets and the percentage of data points reported for each sub-range of hydraulic diameters.

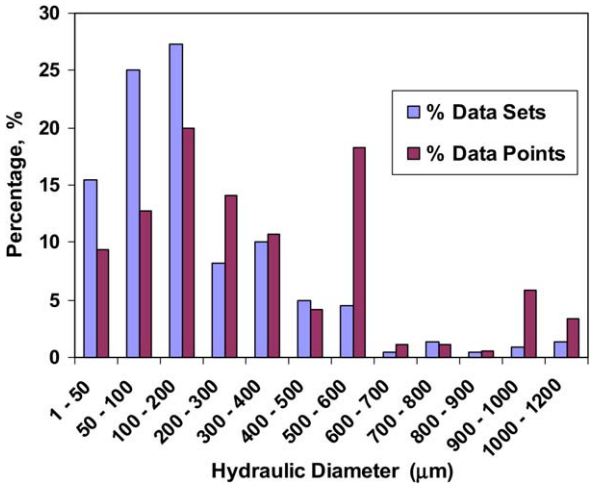

Fig. 1. Distribution of data sets and data points for the range of hydraulic diameters.

The papers used in the present work are shown in Table 1. The ranges of the important microchannel fluid flow parameters are reported. Not all of the parameters were reported by the authors. As a result, some of the parameters are calculated by the present authors using the data from the paper. The present work includes both adiabatic and diabatic works with several different channel geometries.

The Reynolds numbers investigated versus the hydraulic diameters reported are plotted in Fig. 2. The general trend seen

Table 1
Selected literature for single-phase liquid flow in microchannel passages

Author	Year	Fluid/ Shape*	D_h (μm)	$\alpha_c = a/b$	Re	$f\,Re$	C^*	L/D_h	Adiab/ diab**	Account losses	Agree laminar
Tuckerman and Pease, [4]	1981	water / R	92–96	0.17–0.19	291–638	14.0–20.8	0.73–1.06	104–109	D	N	Y
Missaggia et al., [5]	1989	water / R	160	0.25	2350	611.6	33.54	6	D	N	N
Riddle et al., [6]	1991	water / R	86–96	0.06–0.16	96–982	15.8–80.6	0.79–4.06	156–180	D	N	N
Rahman and Gui, [7]	1993	water / R	299–491	3.00–6.00	275–3234	2279.8–8720.2	121.89 -507.10	94–154	D	N	N
Rahman and Gui, [8]	1993	water, R11 / R	299–491	3.00–6.00	275–3234	2279.8–8720.2	121.89 -507.10	94–154	D	N	N
Gui and Scaringe, [9]	1995	water / Tr	338–388	0.73–0.79	834–9955	18.4–76.8	1.28–5.33	119–136	D	N	N
Peng et al., [10]	1995	methanol / R	311–646	0.29–0.86	1530–13455	ID	ID	70–145	D	N	N
Peng and Peterson, [11]	1995	water / R	311	0.29	214–337	ID	ID	145	D	N	N
Cuta et al., [12]	1996	R124 / R	425	0.27	101–578	7.0–36.6	0.39–2.04	48	D	Y	Y
Peng and Peterson, [13]	1996	water / R	133–200	0.5–1.0	136–794	192.1–394.1	13.50–27.70	25–338	D	N	N
Jiang et al., [14]	1997	water / C, Tr	8–68	0.38–0.44	0.032–26.1	3.6–48.9	0.22–3.05	69–276	D	N	Y
Tso and Mahulikar, [15]	1998	water / C	728	NA	16.6–37.5	ID	ID	76–89	D	Y	N
Vidmar and Barker, [16]	1998	water / C	131	NA	2452–7194	28.4–89.2	1.77–5.58	580	D	Y	Y
Adams et al., [17]	1999	water / Tr	131	ID	3899–21429	ID	ID	141	D	Y	Y
Mala and Li, [18]	1999	water / C	50–254	NA	132–2259	22.2–321.2	1.38–20.07	150–490	A	Y	Y
Papautsky et al., [19]	1999	water / R	44–47	5.69–26.42	0.002–4	19.8–32.1	0.98–1.41	164–177	A	Y	Y
Pfund et al., [20]	2000	water / R	253–990	19.19–78.13	55.3–3501	21.9–40.7	0.01–1.81	101–396	A	Y	Y
Qu et al., [21]	2000	water / Tr	51–169	1.54–14.44	6.2–1447	9.2–36.7	0.55–1.68	165–543	A	Y	Y
Qu et al., [22]	2000	water / Tr	62–169	2.16–11.53	94–1491	ID	ID	178–482	D	N	N
Rahman, [23]	2000	water / R	299–491	3.00–6.00	275–3234	9119.2–34880.6	487–2028	94–154	D	N	N
Xu et al., [24]	2000	water / R	30–344	0.58–24.53	5–4620	9.1–46.2	0.53–3.18	145–1070	A	Y	Y
Chung et al., [25]	2002	water / C	100	NA	1.9–3237	41.2–33.3	0.89–2.08	875	A	Y	Y
Judy et al., [26]	2002	water, methanol, isopropyl / C, R	14–149	1.00	7.6–2251	12.9–20.3	0.83–1.27	1203–5657	A	Y	Y
Lee et al., [27]	2002	water / R	85	0.25	119–989	19.4–43.6	1.06–2.39	118	D	Y	Y
Qu and Mudawar, [28]	2002	water / R	349	0.32	137–1670	12.1–33.4	0.70–1.94	128	D	Y	Y
Bucci et al., [29]	2003	water / C	172–520	NA	2–5272	14.0–51.9	0.87–3.24	ID	D	Y	Y
Jung and Kwak, [30]	2003	water / R	100–200	1.00–2.00	50–325	10.7–33.4	0.69–2.15	75–150	D	Y	Y
Lee and Garimella, [31]	2003	water / R	318–903	0.17–0.22	558–3636	ID	ID	28–80	D	Y	Y
Park et al., [32]	2003	water / R	73	4.44	4.2–19.1	ID	ID	654	D	–	–
Tu and Hrnjak, [33]	2003	R134a / R	69–305	4.11–11.61	112–3500	17.6–50.5	0.89–2.35	131–288	D	Y	Y
Wu and Cheng, [34]	2003	water / Tr, Ti	26–291	ID	11.1–3060	11.7–31.6	0.73–1.98	ID	A	Y	Y
Wu and Cheng, [35]	2003	water / Tr	169	1.54–26.20	16–1378	8.6–34.1	0.58–1.88	192–467	D	N	Y
Baviere et al., [36]	2004	water / R	14–593	83.33	0.1–7985	21.5–71.8	0.91–3.04	138–429	D	Y	Y
Hsieh et al., [37]	2004	water / R	146	1.74	45–969	14.6–51.2	0.96–3.39	164	D	Y	Y
Owhaib and Palm, [38]	2004	R134a / C	800–1700	NA	1262–16070	ID	ID	191–406	D	Y	Y

NA = Not Applicable, ID = Insufficient Data; *C = circular, R = rectangular, Tr = trapezoid, Ti = triangle; **A = Adiabatic, D = Diabatic; ***Y = Yes, N = No

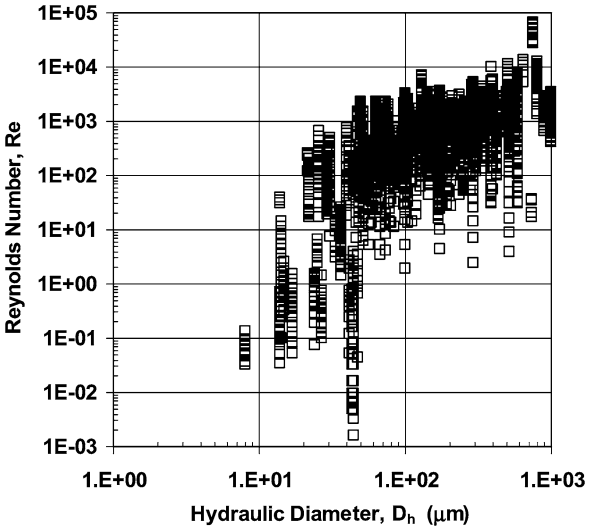

Fig. 2. Reynolds number vs. hydraulic diameters for the selected data sets.

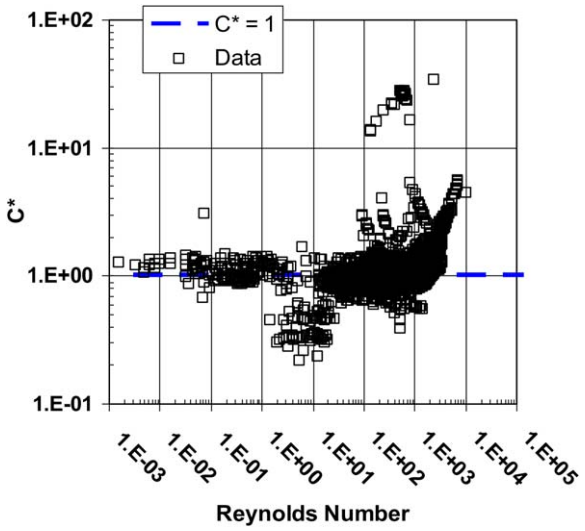

Fig. 3. Non-dimensional Poiseuille number vs. Reynolds number for all of the data sets.

in the figure is that as the hydraulic diameter decreases the Reynolds number also decreases. This makes sense because the pressure drop increases sharply as the hydraulic diameter is reduced and lower flow rates are employed. There are data for very low Reynolds numbers, for laminar Reynolds numbers, and for transitional flows. However, there seems to be little to no data for turbulent flows in microchannels.

The channel aspect ratio is reported for each work. There have been several different definitions for channel aspect ratio in literature. For the present work, the channel aspect ratio, α_c is defined in Eq. (1).

$$\alpha_c = \frac{a}{b} \tag{1}$$

It is defined as the channel width, a, divided by the channel height, b. The channel orientation in the microchannel heat exchanger is not critical for fluid flow as the cross-sectional flow area is of primary concern. However, the orientation of the geometry and the applied boundary conditions are crucial for heat transfer. It would be desirable to have several deep, narrow (i.e. $\alpha_c < 1.0$) microchannels than to have a few wide, shallow microchannels. Given an adiabatic top, the deeper microchannels would have a larger heat transfer area versus the shallower ones and thus better performance.

The most common observation of discrepancy noted by researchers is an early departure from the laminar theory that suggests a lower critical Reynolds number. The $f\,Re$ number is non-dimensionalized using the theoretical value of $f\,Re$ and is given by:

$$C^* = \frac{(f\,Re)_{\text{exp}}}{(f\,Re)_{\text{theory}}} \tag{2}$$

where $f\,Re_{\text{exp}}$ is the experimentally determined value and $f\,Re_{\text{theory}}$ is the theoretical value determined by the channel geometry. It would be more appropriate to evaluate the C^* ratio for each geometry.

Fig. 3 shows the C^* ratio versus Reynolds number for all of the available data sets. There are several data sets that show good agreement and there are several data sets that show a great deal of discrepancy. This fact leads to the current dilemma of questioning conventional theory in microchannel flows.

There seems to be a common thread between all of the papers that have reported some form of discrepancy between the experimental data and the predicted theoretical values. Those authors that have not discussed the entrance and exit losses or the developing length seem to be the same authors reporting the discrepancies. The authors that have removed the added pressure drop for the entrance and exit and the added friction factor for the developing region also report good agreement with the predicted theory.

Table 1 presents information on if the authors have accounting for the losses or the developing region in their test sections. However, it is possible to have an entrance condition and a flow case that would give good agreement with theoretical predictions. Nevertheless, it seems that this is the common occurrence. If the papers that do not account for these effects on friction factor are removed, the database shows reasonably good agreement with predicted theory.

Fig. 4 shows the C^* ratio for the reduced data set. The reported discrepancies in f are removed from the data when losses and developing flow is considered. This makes sense because both would be components of pressure drop that would serve to add to the overall pressure drop and artificially increase the friction factor. However, there is still some significant deviation from the desired value of $C^* = 1.0$. When error bounds are applied to Fig. 4, the majority of the data falls between $0.6 < C^* < 1.4$. An explanation of this behavior could come from experimental uncertainties, which will be described in the uncertainty section.

Three papers have been identified to demonstrate agreement with theory over the range of Reynolds numbers and a variety of shapes. Figs. 5, 6 and 7 have been plotted using the same axis to allow for direct comparison.

Fig. 5 shows the data from Papautsky et al. [19] whom investigated water flow in rectangular channels of hydraulic diameters between 44 and 47 μm. The C^* ratio is bounded by the

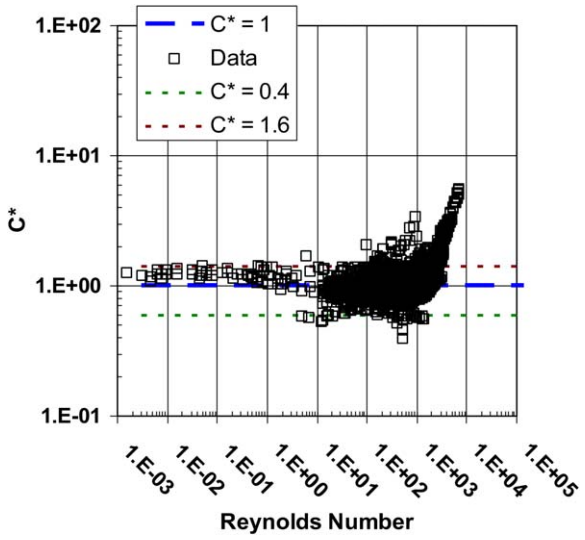

Fig. 4. Non-dimensional Poiseuille number vs. Reynolds number for the reduced data sets.

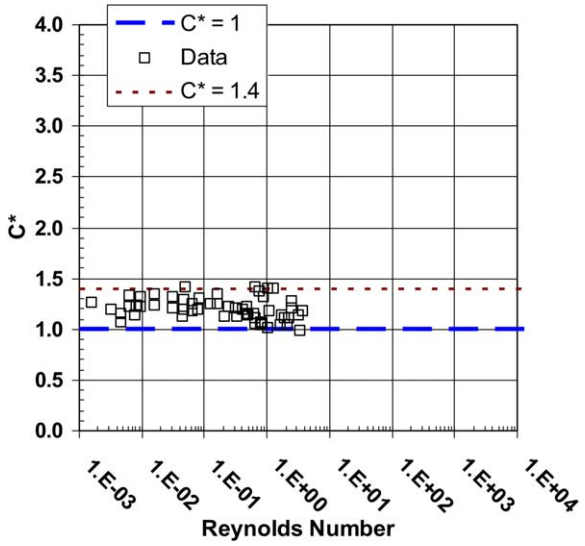

Fig. 5. Non-dimensional Poiseuille number vs. Reynolds number for low laminar Reynolds numbers, Papautsky et al. [19].

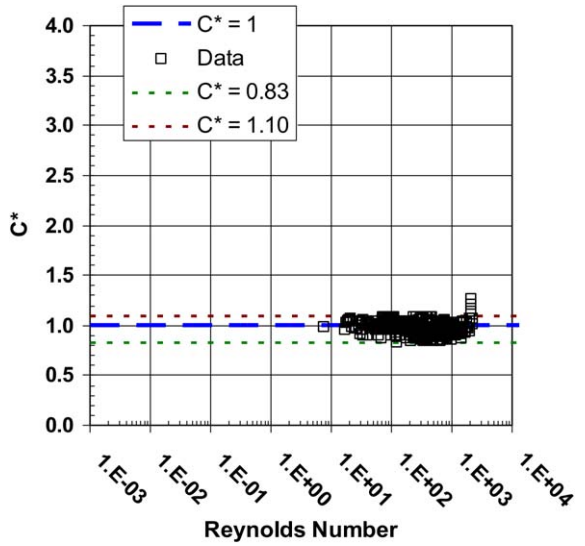

Fig. 6. Non-dimensional Poiseuille number vs. Reynolds number for laminar Reynolds numbers, Judy et al. [26].

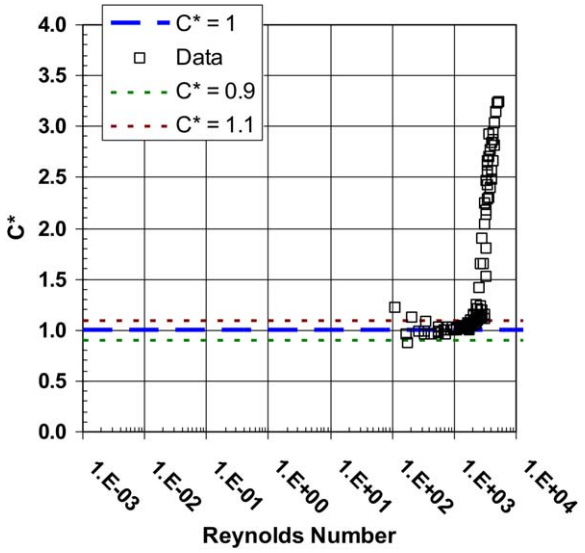

Fig. 7. Non-dimensional Poiseuille number vs. Reynolds number for transitional Reynolds numbers, Bucci et al. [29].

range $1.0 < C^* < 1.4$, which translates into an uncertainty of +40%. The channel diameter is very small and the Reynolds numbers are very low. The experimental uncertainties will be quite large for low Reynolds numbers.

Fig. 6 shows data from Judy et al. [26] whom used water flowing in the laminar Reynolds number range through circular and rectangular tubes with hydraulic diameters between 14 to 149 μm. There is excellent agreement with the C^* ratio being bounded by −15% and +10%. The Reynolds numbers and the channel hydraulic diameters are larger here and the uncertainty is improving.

Finally, Fig. 7 shows the data from Bucci et al. [29] who used water flowing in the transitional Reynolds number range through circular tubes with hydraulic diameters ranging between 172 and 520 μm. Here, the C^* ratio is bounded by ±10%. The channel diameters here are greater than 500 μm at times with larger Reynolds numbers. There is excellent agreement in the laminar region.

All three figures serve to demonstrate the changes in experimental uncertainties with flow range. Although some of those authors did not directly site uncertainties, the scatter in their data may be attributed to the experimental uncertainties. The uncertainties are decreasing with an increase in Reynolds numbers. In several recent papers, the researchers have been more careful with the additional losses seen in complicated flow structures used in microchannels, and as a result, are reporting better agreement with conventional theory. However, it is important to explain the reasons for the discrepancies that exist in the previous literature.

3. Friction factor theory

The present work focuses on the flow of single-phase liquids in microchannel passages. The compressibility effects, slip boundary condition, and the rarefied flow concerns do not apply for these single-phase liquid flows in microchannels. For the present work, it will be assumed that the continuum assumption is valid for microchannels larger than 1.0 μm in hydraulic diameter.

The starting point in the theoretical discussion will be the definition of friction factor, f. One complication for determining the friction factor is the two different definitions for f, Darcy and Fanning. For the present work, the Fanning definition of friction factor will be utilized, because it is more convenient when performing diabatic experiments. It takes the same form of the Colburn j factor equation. Therefore, a link between the heat transfer performance and the pressure drop performance is made through the f and j factors. The Fanning friction factor is defined as the ratio of the wall shear stress to the flow kinetic energy per unit volume and is found using Eq. (3).

$$f = \frac{\tau_w}{1/2\rho \overline{V}^2} \tag{3}$$

where f is the Fanning friction factor, τ_w is the wall shear stress, ρ is the fluid density, and $\overline{V}$ is the average velocity. The friction factor in terms of the pressure drop and mass flux is given by:

$$f = \frac{\rho \Delta p D_h}{2LG^2} \tag{4}$$

where Δp is the pressure drop, D_h is the hydraulic diameter, L is the passage length, and G is the mass flux. For laminar flow, the Poiseuille number, $Po = f\,Re$, is constant. The $f\,Re$ is 16 for a circular passage. The Poiseuille number is a function of aspect ratio for a rectangular passage. It can be determined using Eq. (5) from Shah and London [39].

$$f\,Re = 24\begin{pmatrix} 1 - 1.3553\alpha_c + 1.9467\alpha_c^2 \\ -1.7012\alpha_c^3 + 0.9564\alpha_c^4 \\ -0.2537\alpha_c^5 \end{pmatrix} \tag{5}$$

where α_c is the channel aspect ratio. One constraint for this equation is that the aspect ratio must be less than one. If the channel aspect ratio is greater than 1.0, the inverse is taken to use with Eq. (5).

The turbulent regime has several possible correlations to choose from. Blasius for the smooth round tube correlation is shown in Eq. (6).

$$f = \frac{0.0791}{Re^{1/4}} \tag{6}$$

This correlation is valid for the range of $2,100 < Re < 10^5$ and for e/D ratios $< 1 \times 10^{-6}$.

The pioneering work of Nikuradse [40] varied the roughness of pipes using sand adhered to the walls using a lacquer. He determined the dependence of friction factor upon a non-dimensional wall roughness as seen in Eq. (7).

$$\frac{1}{\sqrt{f}} = 3.48 - 1.737\ln\left(\frac{e}{D}\right) \tag{7}$$

for e/D ratios $> 1 \times 10^{-6}$, the friction factor can also be determined by using the implicit Colebrook [41] equation shown in Eq. (8).

$$\frac{1}{\sqrt{f}} = 3.48 - 1.7372\ln\left\{\frac{e}{D} + \frac{9.35}{Re\sqrt{f}}\right\} \tag{8}$$

This widely accepted correlation is the basis for the turbulent region in the Moody [42] diagram. There are several explicit correlations that demonstrate good agreement with the Colebrook equation. Each have different accuracies and intended ranges. However, the available correlations are derived using rough circular tubes.

The above equations are valid for both adiabatic and diabatic flows. There is often a very large temperature gradient occurring in a boundary layer that is quite large, compared to conventional channels, affecting the temperature dependent properties. The property ratio method for viscosity given in Kakaç et al. [43] is given in Eq. (9)

$$\frac{f}{f_{cp}} = \left(\frac{\mu_b}{\mu_w}\right)^m \tag{9}$$

where f_{cp} is the constant property friction factor, f is the property corrected friction factor, μ_b is the viscosity of the fluid calculated at the bulk fluid temperature, μ_w is the viscosity of the fluid calculated at the wall temperature, and $m = -0.58$ for laminar heating in a fully developed, circular duct.

4. Hydrodynamically developing flow

The hydrodynamically developing flow can become quite important in microchannels. Due to the often short lengths, the developing flow could dominate the entire flow length of the microchannel. First, the definition of a non-dimensional flow distance is defined in Eq. (10).

$$x^+ = \frac{x}{D_h \cdot Re} \tag{10}$$

where x^+ is the non-dimensional flow distance and x is the axial flow direction location. It is commonly accepted that for a value of $x^+ = 0.05$, the flow can be considered fully developed.

When considering the developing flows, the pressure drop is now related to an apparent friction factor and is seen in Eq. (11), Kakaç et al. [43].

$$\Delta p = \frac{2(f_{app}\,Re)\mu \overline{V} x}{D_h^2} \tag{11}$$

where f_{app} is the apparent friction factor, μ is the viscosity, and x is the axial location of interest. If the entire length of the microchannel is considered, the x term can be the microchannel length.

The apparent friction factor consists of two components. The first is the friction factor from the theory for the fully developed flow and the second is the pressure defect (a.k.a. Hagenbach factor) as given by Eq. (12).

$$\Delta p = \frac{2(f\,Re)\mu V L}{D_h^2} + \frac{\kappa(x)\rho \overline{V}^2}{2} \tag{12}$$

where κ is the Hagenbach factor given by:

$$\kappa(x) = (f_{\text{app}} - f_{\text{FD}})\frac{4 \cdot x}{D_{\text{h}}} \tag{13}$$

The Hagenbach factor will begin at a value of 0 and increase to some fully developed constant value $K(\infty)$. Hagenbach factor has a dependence upon channel aspect ratio for rectangular channels. Eq. (14), with an accuracy of 0.04%, determines the fully developed Hagenbach factor for a rectangular channel.

$$\kappa(\infty) = \begin{pmatrix} 0.6796 + 1.2197\alpha_{\text{c}} + 3.3089\alpha_{\text{c}}^2 \\ -9.5921\alpha_{\text{c}}^3 + 8.9089\alpha_{\text{c}}^4 \\ -2.9959\alpha_{\text{c}}^5 \end{pmatrix} \tag{14}$$

5. Pressure drop measurements in microchannel flows

There are several issues that need to be addressed when performing pressure drop measurements in microchannel flows. Generally, there are three main components that contribute to the overall pressure drop. The inlet and exit losses need to be quantified for the microchannel. The hydrodynamic developing length needs to be carefully evaluated. Finally, the remaining length will have the fully developed frictional loss.

Based upon the reviewed literature, the most common method to measure the pressure drop involves making pressure measurements inside the inlet and outlet manifolds. The different components of pressure that make up the entire pressure drop are shown in Fig. 8. The inlet and outlet loss coefficients are represented by κ_{i} and κ_{o}. The friction factor is higher in the developing flow region. Finally, beyond the entry region, the conventional theory for fully developed flow should apply. The components of the total pressure drop can be seen in Eq. (15).

$$\Delta p = \frac{\rho \cdot \overline{V}^2}{2}\left[\kappa_{\text{i}} + \kappa_{\text{o}} + \frac{f_{\text{app}} \cdot L}{D}\right] \tag{15}$$

where κ_{i} is the inlet loss coefficient and κ_{o} is the outlet loss coefficient. The friction factor used in Eq. (11) is the apparent friction factor and accounts for the developing region.

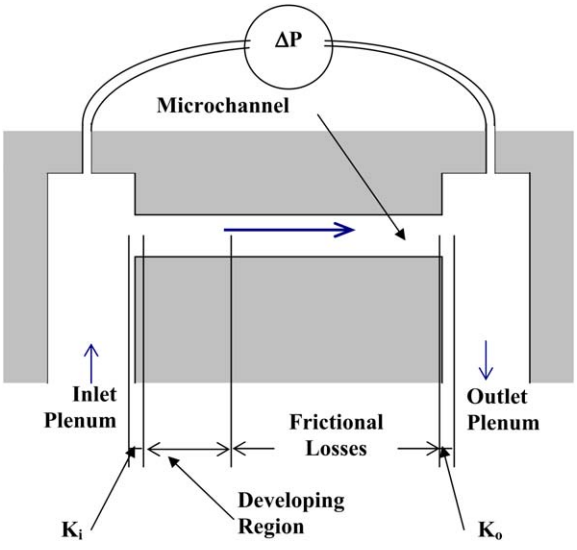

Fig. 8. Components of pressure when measuring Δp in microchannel manifolds.

Eqs. (12) and (15) can be combined to calculate the total pressure drop. Eq. (16) shows all of the components in the total pressure drop measurement.

$$\Delta p_{\text{tot}} = \frac{\kappa_{\text{i}}\rho\overline{V}^2}{2} + \frac{\kappa_{\text{o}}\rho\overline{V}^2}{2} + \frac{2(f\,Re)\mu\overline{V}L}{D_{\text{h}}^2} + \frac{\kappa(x)\rho\overline{V}^2}{2} \tag{16}$$

The first two terms represent the inlet and exit losses, respectively. The third term is the frictional losses resulting from the fully developed flow. The last term represents the added pressure drop due to the developing flow region.

Fortunately, the entrance and exit losses can be eliminated to generate fundamental data. Several researchers have addressed this issue. The unknown entrance and exit losses can be eliminated by using two different flow lengths. Bucci et al. [29] measured the overall pressure drop in stainless steel capillary tubes. They used a short length and a long length of tube with the same entrance conditions. Therefore, the entrance and exit losses are the same for each flow case and can be eliminated.

Tu and Hrnjak [33] fabricated a test section from clear polyvinylchloride (PVC). There were two pressure taps located over the microchannel and away from the inlet and exit manifolds. Baviere et al. [36] fabricated a microchannel with local pressure channels away from the inlet and exit plenums in a silicon substrate. The pressure transducers, fabricated from a thin silicon membrane, were also incorporated into the silicon substrate. Each of these works reported agreement with conventional theory. Kandlikar et al. [44] also made local pressure measurements in an aluminum channel. They reported agreement with conventional theory for the smooth channels.

For a conventional system, the inlet and exit plenums are sufficiently large in area to cause the flow to have a very low velocity and create a smooth inlet. The entrance condition for a microchannel could be considerably more complex. If the plenums are not properly sized, an added component of dynamic pressure could be included in the pressure drop measurements. A verification of the losses in the plenum would be appropriate.

6. Experimental uncertainties in microchannels

The experimental uncertainties can become quite large for a microchannel heat exchanger. The physical size of the system being measured is a complication. The magnitudes of the measurements can become a problem as well.

Fortunately, several of the standards for experimental uncertainties still apply in the microscale. The two best standards for determining experimental uncertainties are ASME PTC 19.1 [45] and NIST Technical Note 1297 [46]. There are many similarities between these standards and many others. In general, the total uncertainty is comprised of two parts; bias error and precision error as given:

$$U = 2\sqrt{\left(\frac{B}{2}\right)^2 + \left(\frac{\sigma}{\sqrt{N}}\right)^2} \tag{17}$$

where U is the total uncertainty, B is the bias error, σ is the standard deviation, N is the number of samples. The bias error

is a measure of the systematic error and the precision error is a measure of the random errors in the system.

When propagating errors, Eq. (18) gives the uncertainty of a calculated parameter based upon the measured variables.

$$U_p = \sqrt{\sum_{i=1}^{n}\left(\frac{\partial p}{\partial a_i}u_{ai}\right)^2} \tag{18}$$

where p is the calculated parameter, a_i is a variable used to calculate p, and u_{ai} is the uncertainty of the variable a_i. The uncertainty in any parameter is the sum of the uncertainties of the components used to calculate that parameter.

As stated previously, it seems that the vast majority of data can be bounded by $0.6 < C^* < 1.4$. This translates into an uncertainty of $\pm 40\%$. Although this value might appear rather large, for some of the experimental data sets it would actually be consistent with their associated uncertainties. Eq. (19) shows the propagated error for the $f\,Re$ product, in terms of fractional uncertainties.

Several authors have discussion experimental uncertainties in their papers. This is similar to the results found by Judy et al. [26]. They demonstrated that with some assumptions about the flow and flow regime, the uncertainty is dominated by $4 \times D_h$, compared to other measurements.

$$\frac{U_{f\,Re}}{f\,Re} = \left[\left(\frac{U_\rho}{\rho}\right)^2 + \left(\frac{U_{\Delta p}}{\Delta p}\right)^2 + \left(\frac{U_{D_h}}{D_h}\right)^2 + \left(\frac{U_L}{L}\right)^2 + 2\left(\frac{U_G}{G}\right)^2 + \left(\frac{U_{Re}}{Re}\right)^2\right]^{1/2} \tag{19}$$

It would be beneficial to determine the experimental uncertainty of $f\,Re$ based upon actual measured parameters. The expanded uncertainty expression for $f\,Re$, based upon measured variables is given by Eq. (20).

$$\frac{U_{f\,Re}}{f\,Re} = \left[2\left(\frac{U_\rho}{\rho}\right)^2 + \left(\frac{U_\mu}{\mu}\right)^2 + \left(\frac{U_{\Delta p}}{\Delta p}\right)^2 + \left(\frac{U_L}{L}\right)^2 + 3\left(\frac{U_Q}{Q}\right)^2 + 5\left(\frac{U_a}{a}\right)^2 + 5\left(\frac{U_b}{b}\right)^2 + 2\left(\frac{U_a}{a+b}\right)^2 + 2\left(\frac{U_b}{a+b}\right)^2\right]^{1/2} \tag{20}$$

where Q is the volumetric flow rate. The equation presents the uncertainty in $f\,Re$ in actual measured variables and as such, terms such as the $a+b$ in the denominator are derived from the propagation of the hydraulic diameter measurements. It can be seen that the most dominant terms in the $f\,Re$ uncertainty are the measurements of microchannel width and height, and the flow rate. Therefore, even with the most careful pressure drop measurements, there is still going to be a large uncertainty due to the measurement errors of the microchannel dimensions and the flow rate. It is entirely plausible that some of the remaining data sets could have experimental uncertainties as high as 40% or higher. In addition, the pressure drop term is actually more complex. The entrance and exit losses will add to the overall uncertainty.

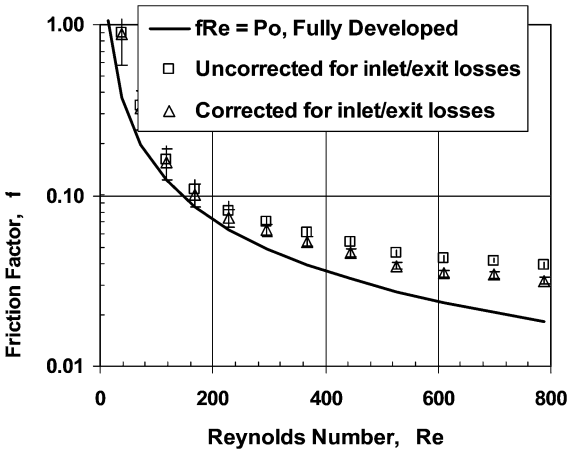

Fig. 9. Apparent friction factor vs. Reynolds number considering entrance and exit losses. Line = theoretical prediction of f, square points = uncorrected data, triangle points = corrected data; Adiabatic; $a = 200$ μm, $b = 250$ μm, $L = 10$ mm.

7. New experimental data

A microchannel with a width of 200 μm, a depth of 250 μm, and a length of 10 mm is used to provide new experimental data to illustrate the different components of the total pressure drop measurement. The details of the test section and the experimental facility are described in Steinke et al. [47]. The data presented is for adiabatic, single-phase degassed water and covers the range of Reynolds numbers from 14 to 789. There are 26 parallel channels connected to a common header. The inlet plenum and outlet plenums are in a polycarbonate cover plate. The temperature and pressure are measured in the plenums. The plenum areas are sufficiently large to ensure measurement of only the static pressure.

The apparent friction factor is calculated from the measured pressure drop. It is plotted versus Reynolds number in Fig. 9. It is compared to the conventional friction factor theory for laminar flow. The data points uncorrected for entrance and exit losses are shown as squares. The experimental uncertainty is calculated and the error bars are included.

There is deviation from the laminar flow theory as observed in the data in the low Reynolds number range. However, the experimental uncertainties are quite large for this flow regime. As the Reynolds number increases, the data begins to show good agreement with the theory. Finally, the data begins to depart from the predicted $f\,Re$ approximately at a Reynolds number of 300. This would suggest early transition to turbulent if a regular friction factor versus Reynolds number plot exhibited this behavior. This is not an accurate representation of the measured pressure drop.

The entrance and exit losses are calculated and subtracted according to Eq. (20). These losses are found using the conventional constriction and expansion area theory. The area ratio changes are used to determine the loss coefficients. The corrected data shows little difference to the uncorrected data in the low Reynolds number region and a more significant change in the higher Reynolds number region. However, this component

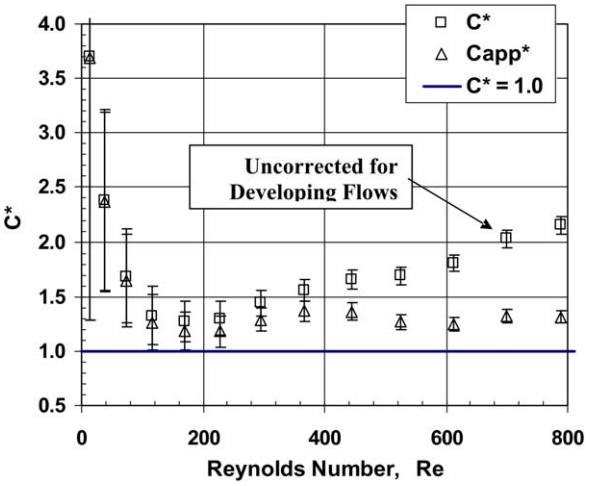

Fig. 10. Apparent C^* ratio vs. Reynolds number considering developing flow. Line = theoretical prediction, square points = uncorrected data, triangle points = corrected data; Adiabatic, $a = 200$ μm, $b = 250$ μm, $L = 10$ mm.

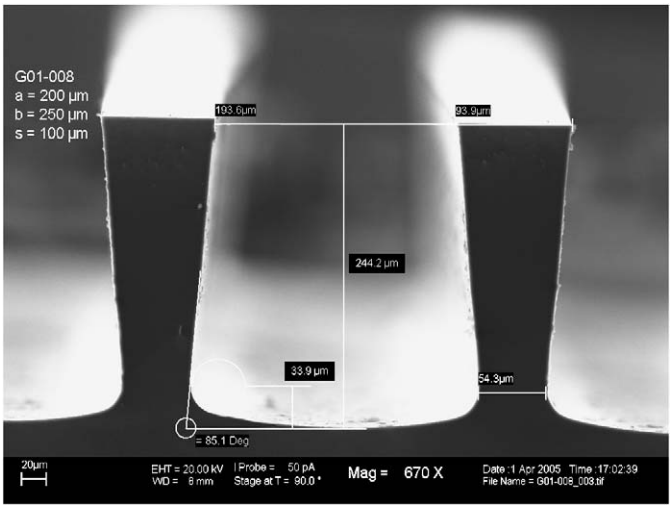

Fig. 11. Actual cross section of tested microchannel. $a = 194$ μm, $b = 244$ μm, $L = 10$ mm, $\theta = 85$ degrees, $D_h = 227$ μm.

alone does not correct enough to demonstrate good agreement with the theory.

The entrance lengths at the higher Reynolds numbers become quite significant. For example, the last data point shown in Fig. 10 has an x^+ of 0.048 at the exit. This means that the entrance length is 9.8 mm and the flow in the microchannel is not quite fully developed at the exit and the entire flow length is developing flow. This must be taken into account when comparing to the theoretical value. Therefore, the apparent friction factor, f_{app}, must be utilized to compare with theory.

The C^* ratio versus Reynolds number is shown in Fig. 10. The C^* ratio would be more appropriate to report for a microchannel geometry of this nature. It will also avoid confusion between the regular friction factor and the apparent friction factor. For comparison purposes, the C^* ratio for the uncorrected data and the C^*_{app} ratio for the data corrected to account for the developing flow portion are presented together.

The uncorrected data begins to rise in value after a Reynolds number of 300. However, the data that is calculating C^* based upon the apparent friction factor continues to show good agreement, within approximately 25% error. Although the data does not match perfectly, there is good general agreement and the trend is properly predicted.

8. Channel geometry evaluation

The channel dimensions have a major effect on the friction factor calculations as seen from Eq. (20). The measurements for the microchannels tested were first made using non-destructive measurement techniques. The dimensions resulting from the optical measurement technique yield a microchannel width of 201 ± 5 μm and a microchannel depth of 247 ± 5 μm. At the completion of the testing, the microchannel test section was cleaved in order to facilitate accurate cross sectional measurements. Upon destruction, the profile of the supposed rectangular microchannels is actually found to be trapezoidal in shape.

Fig. 11 shows an SEM image of the microchannel geometry tested. It can be seen that there is significant undercutting

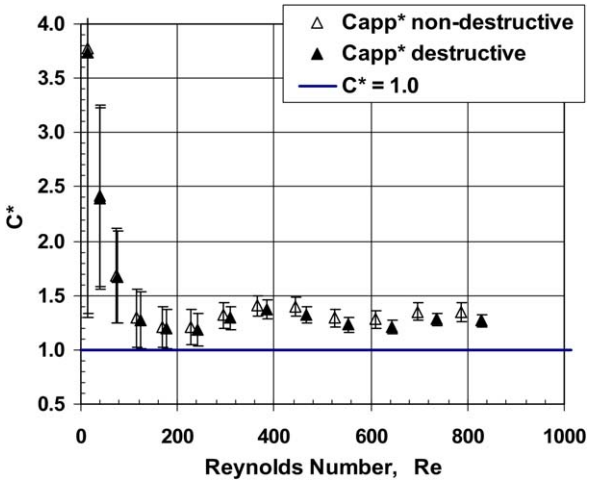

Fig. 12. Apparent C^* ratio vs. Reynolds number considering measured cross section. Line = theoretical prediction, square points = rectangular data, triangle points = trapezoid data; Adiabatic, trapezoid top width =194 μm, height = 244 μm, $L = 10$ mm, $\theta = 85$ degrees.

of the fin area in these microchannels. The width at the top is 194 ± 1 μm. The depth is 244 ± 1 μm with a sidewall angel of 85 degrees. This profile could not be obtained from non-destructive measurement techniques. Over twelve measurements of the height and width are made along the flow length of the microchannel. The mean of those measurements are used to determine the hydraulic diameter.

The microchannel cross section is not a true trapezoid. However, careful measurements are made to determine the cross sectional area and the proper hydraulic diameter is calculated. The equivalent trapezoid has an angle of 85 degrees. The corresponding $f\,Re$ number is 14.5 for trapezoidal ducts with that side wall angle and aspect ratio.

The friction factor is now using the corrected geometry for the new trapezoidal cross section. The apparent C^* is shown in Fig. 12. It can be seen that the data now shows improved agreement with theory when the inlet and exit losses and devel-

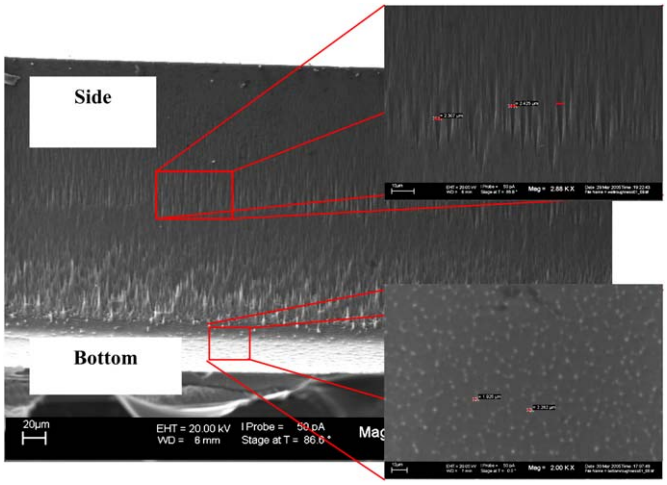

Fig. 13. Surface roughness in the microchannels. Side wall $e/D_h = 0.01$, Bottom wall $e/D_h = 0.007$.

oping flows are accounted for. Using the non-destructive measurement method, the remaining error in the higher Reynolds number range is 33%. After the cross section has been measured using a cut of the test section, the resulting hydraulic diameter is 227 μm and the error is reduced to 24%. In addition to identifying the channel as a trapezoid, the area reduction resulting from the rounded corners was accounted for while calculating the equivalent hydraulic diameter.

The remaining discrepancies can be attributed to using $f\,Re_{app}$ values for a true trapezoidal duct, as no data is available for the trapezoidal geometry with rounded corners. Also, the first order K factors used for inlet and exit losses based upon conventional empirical data can be attributed to the remaining discrepancies.

9. Surface roughness measurements

Finally, the surface roughness of the microchannel walls is another important parameter. In conventional sized channels, the surface roughness has been identified to play a dominate role only in the turbulent region. The data reduced from previous literature suggest the same trend for microchannels. However, this is still an open topic of discussion. It would be important for researchers to report the surface roughness in their work in order to build confidence in that statement.

Fig. 13 shows the nature of the surface roughness in the present microchannel test sections. The pictures of the side wall and bottom wall surfaces showing surface roughness features are obtained using scanning electron microscope (SEM) and are shown in the figure. The majority of the surface has a very small e/D_h ratio, approximately 0.002. The bottom wall does have some roughness features seen in the bottom inset. The average size of those features is 1.5 μm, making the e/D_h ratio approximately 0.007. The side wall has larger roughness features due to the method of fabrication. These features are an artifact of the deep reactive ion etching processes used. The average roughness feature for the side wall is 2.5 μm and the resulting e/D_h ratio is 0.01. The measurement of the surface roughness for future microchannel works should be carefully evaluated.

10. Conclusions

There are over 150 papers specifically addressing the topic of fluid flow and heat transfer in microchannels. Approximately 40 of those papers present useful data on friction factors in microchannels. A database of over 5,000 data points has been generated. The present work includes a Reynolds number range of $0.002 < Re < 5{,}000$ and a hydraulic diameter range of $8 < D_h < 990$ μm.

An explanation for the deviation in data has been presented for the first time. The papers that do not account for the entrance and exit losses or the developing flow in the microchannel are the same papers that report significant deviation from theory. The remaining data sets show agreement with conventional theory. Therefore, the conventional friction factor theory is applicable for the range of Reynolds numbers and hydraulic diameters included.

Experimental uncertainties can become quite large for microchannel heat exchangers. It is demonstrated that the uncertainty in $f\,Re$ is dominated by the microchannel width and height measurements. Even a very accurate pressure drop measurement will often be overshadowed by the geometry measurement uncertainties.

The components that contribute to the total pressure drop occurring across a microchannel heat exchanger are identified. The components include the inlet and outlet losses, the developing flow losses, and the fully developed flow losses.

New experimental data is generated to demonstrate the procedure for correcting the measured pressure drop. First, the data is corrected for inlet and exit losses and then it is corrected for developing flows. The corrected data shows good preliminary agreement in value and trend with the conventional theory for laminar fluid flow.

The microchannel geometry must be carefully evaluated. There is no substitute to accurate measurements obtained through destructive measurement of the channel geometry. The profiles of the flow passage must be carefully determined while reducing the experimental data for obtaining the experimental friction factors.

References

[1] S.G. Kandlikar, W.J. Grande, Evolution of microchannel flow passages – thermohydraulic performance and fabrication technology, Heat Transfer Engrg. 24 (1) (2003) 3–17.

[2] S.G. Kandlikar, W.J. Grande, Evaluation of single phase flow in microchannels for high heat flux chip cooling—thermohydraulic performance enhancement and fabrication technology, Heat Transfer Engrg. 24 (1) (2004) 5–16.

[3] M.E. Steinke, S.G. Kandlikar, Review of single-phase heat transfer enhancement techniques for application in microchannels, minichannels and microdevices, Int. J. Heat Techn. 22 (2) (2004) 3–11.

[4] D.B. Tuckerman, R.F.W. Pease, High-performance heat sinking for VSLI, IEEE Electron Device Lett. EDL-2 (1981) 126–129.

[5] L.J. Missaggia, J.N. Walpole, Z.L. Liau, R.J. Phillips, Microchannel heat sinks for two-dimensional high-power-density diode laser arrays, IEEE J. Quantum Electron. 25 (9) (1989) 1988–1992.

[6] R.A. Riddle, R.J. Contolini, A.F. Bernhardt, Design calculations for the microchannel heatsink, in: Proc. of the Technical Program – National

Electronic Packaging and Production Conference, vol. 1, 1991, pp. 161–171.
[7] M.M. Rahman, F. Gui, Experimental measurements of fluid flow and heat transfer in microchannel cooling passages in a chip substrate, in: Proc. of the ASME International Electronics Packaging Conference, September 29–October 2 1993, Binghamton, NY, USA, ASME publications 4-2, 1993, pp. 685–692.
[8] M.M. Rahman, F. Gui, Design, fabrication, and testing of microchannel heat sinks for aircraft avionics cooling, in: Proc. of the Intersociety Energy Conversion Engineering Conference, vol. 1, 1993, pp. 1–6.
[9] F. Gui, R.P. Scaringe, Enhanced heat transfer in the entrance region of microchannels, in: Proc. of the Intersociety Energy Conversion Engineering Conference, 1995, pp. 289–294.
[10] X.F. Peng, B.X. Wang, G.P. Peterson, H.B. Ma, Experimental investigation of heat transfer in flat plates with rectangular microchannels, Int. J. Heat Mass Transfer 38 (1) (1995) 127–137.
[11] X.F. Peng, G.P. Peterson, Effect of thermofluid and geometrical parameters on convection of liquids through rectangular microchannels, Int. J. Heat Mass Transfer 38 (4) (1995) 755–758.
[12] J.M. Cuta, C.E. McDonald, A. Shekarriz, Forced convection heat transfer in parallel channel array microchannel heat exchanger, in: ASME, HTD, Advances in Energy Efficiency, Heat/Mass Transfer Enhancement, vol. 338, 1996, pp. 17–23.
[13] X.F. Peng, G.P. Peterson, Convective heat transfer and flow friction for water flow in microchannel structures, Int. J. Heat Mass Transfer 39 (12) (1996) 2599–2608.
[14] X.N. Jiang, Z.Y. Zhou, X.Y. Huang, C.Y. Liu, Laminar flow through microchannels used for microscale cooling systems, in: Proc. of the Electronic Packaging Technology Conference, EPTC, 1997, pp. 119–122.
[15] C.P. Tso, S.P. Mahulikar, Multimode heat transfer in two-dimensional microchannel, Am. Soc. Mech. Engineers, EEP 26 (2) (1999) 1229–1233.
[16] R.J. Vidmar, R.J. Barker, Microchannel cooling for a high-energy particle transmission window, an RF transmission window, and VLSI heat dissipation, IEEE Trans. Plasma Sci. 26 (3) (1998) 1031–1043.
[17] T.M. Adams, M.F. Dowling, S.I. Abdel-Khalik, S.M. Jeter, Applicability of traditional turbulent single-phase forced convection correlations to noncircular microchannels, Int. J. Heat Mass Transfer 42 (23) (1999) 4411–4415.
[18] G.M. Mala, D.Q. Li, Flow characteristics of water in microtubes, Int. J. Heat Fluid Flow 20 (2) (1999) 142–148.
[19] I. Papautsky, J. Brazzle, T. Ameel, A.B. Frazier, Laminar fluid behavior in microchannels using micropolar fluid theory, Sensors and Actuators A: Physical 73 (1–2) (1999) 101–108.
[20] D. Pfund, D. Rector, A. Shekarriz, A. Popescu, J. Welty, Pressure drop measurements in a microchannel, AIChE J. 46 (8) (2000) 1496–1507.
[21] W. Qu, M. Mala, D. Li, Heat transfer for water in trapizoid silicon microchannels, Int. J. Heat Mass Transfer 43 (2000) 3925–3936.
[22] W. Qu, G.M. Mala, D. Li, Pressure-driven water flows in trapezoidal silicon microchannels, Int. J. Heat Mass Transfer 43 (3) (2000) 353–364.
[23] M.M. Rahman, Measurements of heat transfer in microchannel heat sinks, Int. Comm. Heat Mass Transfer 27 (4) (2000) 495–507.
[24] B. Xu, K.T. Ooi, N.T. Wong, W.K. Choi, Experimental investigation of flow friction for liquid flow in microchannels, Int. Comm. Heat Mass Transfer 27 (8) (2000) 1165–1176.
[25] P.M.-Y. Chung, M. Kawaji, A. Kawahara, Characteristics of single-phase flow in microchannels, in: Proc. of Fluids Engineering Division Summer Meeting, July 14–18, 2002, Montreal, Quebec, Canada, ASME Publications, 2002, pp. 1219–1227.
[26] J. Judy, D. Maynes, B.W. Webb, Characterization of frictional pressure drop for liquid flows through microchannels, Int. J. Heat Mass Transfer 45 (17) (2002) 3477–3489.
[27] P.S. Lee, J.C. Ho, H. Xue, Experimental study on laminar heat transfer in microchannel heat sink, in: The Eighth Intersociety Conference on Thermal and Thermomechanical Phenomena in Electronic Systems, 30 May–1 June 2002, ITHERM 2002, IEEE Publications, 2002, pp. 379–386.
[28] W. Qu, I. Mudawar, Experimental and numerical study of pressure drop and heat transfer in a single-phase micro-channel heat sink, Int. J. Heat Mass Transfer 45 (12) (2002) 2549–2565.
[29] A. Bucci, G.P. Celata, M. Cumo, E. Serra, G. Zummo, Water single-phase fluid flow and heat transfer in capillary tubes, in: Int. Conference on Microchannels and Minichannels, Paper # 1037, ASME, vol. 1, 2003, pp. 319–326.
[30] J.-Y. Jung, H.-Y. Kwak, Fluid flow and heat transfer in microchannels with rectangular cross section, in: Int. Conference on Microchannels and Minichannels, Paper # 1032, vol. 1, 2003, pp. 291–297.
[31] P.-S. Lee, S.V. Garimella, Experimental investigation of heat transfer in microchannels, in: Proceedings of the ASME Summer Heat Transfer Conference, 2003, pp. 391–397.
[32] H. Park, J.J. Pak, S.Y. Son, G. Lim, I. Song, Fabrication of a microchannel integrated with inner sensors and the analysis of its laminar flow characteristics, Sensors and Actuators A: Physical 103 (3) (2003) 317–329.
[33] X. Tu, P. Hrnjak, Experimental investigation of single-phase flow pressure drop through rectangular microchannels, in: Int. Conference on Microchannels and Minichannels, Paper # 1028, ASME Publications, vol. 1, 2003, pp. 257–267.
[34] H. Wu, P. Cheng, An experimental study of convective heat transfer in silicon microchannels with different surface conditions, Int. J. Heat Mass Transfer 46 (14) (2003) 2547–2556.
[35] H. Wu, P. Cheng, Friction factors in smooth trapezoidal silicon microchannels with different aspect ratios, Int. J. Heat Mass Transfer 46 (14) (2003) 2519–2525.
[36] R. Baviere, F. Ayela, S. Le Person, M. Favre-Marinet, An experimental study of water flow in smooth and rough rectangular micro-channels, in: Int. Conference on Microchannels and Minichannels, ASME Publications, 2004.
[37] S.-S. Hsieh, C.-Y. Lin, C.-F. Huang, H.-H. Tsai, Liquid flow in a microchannel, J. Micromech. Microengrg. 14 (4) (2004) 436–445.
[38] W. Owhaib, B. Palm, Experimental investigation of single-phase convective heat transfer in circular microchannels, Exp. Thermal Fluid Sci. 28 (2–3) (2004) 105–110.
[39] R.K. Shah, A.L. London, Laminar Flow Forced Convection in Ducts, Adv. Heat Transfer, Supplement 1, Academic Press, New York, 1978.
[40] J. Nikuradse, Strmungsgesetze in rauhen Rohren, V.D.I. Forschungsheft 361 (1933) 1–22.
[41] C.F. Colebrook, Turbulent flow in pipes with particular reference to the transition region between the smooth and rough pipe laws, J. Institution of Civil Engineers, London 11 (1938–1939) 133–156.
[42] L.F. Moody, Friction factors for pipe flow, Trans. ASME 66 (8) (1944) 671–684.
[43] S. Kakaç, R.K. Shah, W. Aung, Handbook of Single-Phase Convective Heat Transfer, John Wiley & Sons, New York, 1987.
[44] S.G. Kandlikar, D. Schmitt, A.L. Carrano, J.B. Taylor, Characterization of surface roughness effects on pressure drop in single-phase flow, Phys. Fluids 17 (10) (2005).
[45] ASME PTC 19.1, 1998.
[46] NIST Technical Note 1297, 1994.
[47] M.E. Steinke, S.G. Kandlikar, J.H. Magerlein, E.G. Colgan, A.D. Raisanen, Development of an experimental facility for investigating single-phase liquid flow in microchannels, Heat Transfer Engrg. 27 (4) (2006) 1–12.